ISSN 1674-1056
http://cpb.iphy.ac.cn
http://iopscience.iop.org/cpb
中国物理 B
Chinese Physics
中国物理
Chinese Physics B

Nonlinear continuous bi-inductance electrical line with dissipative elements: Dynamics of the low frequency modulated waves

S M Ngounou, F B Pelap

Citation: Chin. Phys. B . 2020, 29(4): 040502 . **doi:** 10.1088/1674-1056/ab75d6
Journal homepage: http://cpb.iphy.ac.cn; http://iopscience.iop.org/cpb

What follows is a list of articles you may be interested in

Dynamical response of a neuron-astrocyte coupling system under electromagnetic induction and external stimulation

Zhi-Xuan Yuan(袁治轩), Pei-Hua Feng(冯沛华), Meng-Meng Du(独盟盟), Ying Wu(吴莹)
Chin. Phys. B . 2020, 29(3): 030504 . **doi:** 10.1088/1674-1056/ab7441

Dynamics of the plane and solitary waves in a Noguchi network: Effects of the nonlinear quadratic dispersion

S A T Fonkoua, M S Ngounou, G R Deffo, F B Pelap, S B Yamgoue, A Fomethe
Chin. Phys. B . 2020, 29(3): 030501 . **doi:** 10.1088/1674-1056/ab696a

Quantum-classical correspondence and mechanical analysis ofa classical-quantum chaotic system

Haiyun Bi(毕海云), Guoyuan Qi(齐国元), Jianbing Hu(胡建兵), Qiliang Wu(吴启亮)
Chin. Phys. B . 2020, 29(2): 020502 . **doi:** 10.1088/1674-1056/ab6205

Effect of magnetic flow and external forcing current on mixed bursting in the pre-Bötzinger complex

Dou-Dou Guo(郭豆豆), Zhuo-Sheng Lü(吕卓生)
Chin. Phys. B . 2019, 28(11): 110501 . **doi:** 10.1088/1674-1056/ab43b9

Chaotic analysis of Atangana-Baleanu derivative fractional order Willis aneurysm system

Fei Gao(高飞), Wen-Qin Li(李文琴), Heng-Qing Tong(童恒庆), Xi-Ling Li(李喜玲)
Chin. Phys. B . 2019, 28(9): 090501 . **doi:** 10.1088/1674-1056/ab38a4

Nonlinear continuous bi-inductance electrical line with dissipative elements: Dynamics of the low frequency modulated waves

S M Ngounou[1,2] and F B Pelap[1,†]

[1] Unité de Recherche de Mécanique et de Modélisation des Systèmes Physiques (UR-2MSP), Faculté des Sciences, Université de Dschang, BP 69 Dschang, Cameroun

[2] Unité de Recherche de Matière Condensée d'Electronique et de Traitement du Signal (UR-MACETS), Faculté des Sciences, Université de Dschang, BP 67 Dschang, Cameroun

(Received 1 January 2020; revised manuscript received 22 January 2020; accepted manuscript online 13 February 2020)

The dynamics of modulated waves in a nonlinear bi-inductance transmission line with dissipative elements are examined. We show the existence of two frequency modes and carry out intensive investigations on the low frequency mode. Thanks to the multiple scales method, the behavior of these waves is investigated and the dissipative effects are analyzed. It appears that the dissipation coefficient increases with the carrier wave frequency. In the continuous approximation, we derive that the propagation of these waves is governed by the complex Ginzburg–Landau equation instead of the Korteweg–de-Vries equation as previously established. Asymptotic studies of the dynamics of plane waves in the line reveal the existence of three additional regions in the dispersion curve where the modulational phenomenon is observed. In the low frequency mode, we demonstrate that the network allows the propagation of dark and bright solitons. Numerical findings are in perfect agreement with the analytical predictions.

Keywords: dissipative bi-inductance network, low frequency mode, continuous approximation, complex Ginzburg–Landau equation

PACS: 05.45.–a, 05.45.Yv **DOI:** 10.1088/1674-1056/ab75d6

1. Introduction

Formation, propagation, interaction of modulated waves and related properties in various nonlinear dispersive media have been subjects of intensive studies.[1] The present study of nonlinear electrical transmission lines (NLTLs) is motivated by their universality. Since the pioneering work of Hirota and Suzuki[2] on electrical lines, the growing interest in the use of NLTLs can be justified by two factors. Firstly, these lines are suitable implements to study wave propagation in nonlinear dispersive media[3] with applications in signal processing and microwaves range.[4] In fact, Nejoh found the envelope soliton of the electron plasma wave in a nonlinear dispersive transmission line.[5] Recently, Makenne *et al.* simulated periodic and chaotic movements of plants subjected to the wind action based on electrical lines.[6] Similarly, Ndzana *et al.* also studied the dynamics of ionic waves in a microtubule modeled by a nonlinear resistor, inductor, and capacitor (*RLC*) transmission line.[7] Secondly, NLTLs possess the capacity to support localized disturbances which act somewhat like particles and are known as solitons.[8] Qualitatively, the origin of soliton in NLTLs is explained by the balance between the effects of dispersion (due to the periodic location of the capacitor in the nonlinear electrical lines) which tends to spread out the wave and nonlinearity (due to the voltage dependence of the capacitance) that leads to the compression of a packet wave.[9] Furthermore, envelope solitons can also be viewed as the result of an instability that leads to a self-induced modulation of the steady state: this phenomenon is well-known as the modulational instability (MI).[10–12]

Despite this great interest in NLTLs and their wide range of applications, two great insufficiencies are noted. First, in the real media, dissipative effects coexist with nonlinear and dispersive effects and may intervene in the wave generation and its propagation. But, only few works analyzed these dissipative effects in the NLTLs. Indeed, Yemele *et al.* investigated analytically the dynamics of modulated waves in a nonlinear *LC* transmission line with dissipative elements and derived the damped nonlinear Schrödinger equation as the amplitude equation.[13] They showed that the effects of the dissipative losses in the series branch are more manifested than those resulting from the dissipative losses in the shunt branch. Moreover, Ndzana *et al.* exploited a similar dissipative network and established in the semi-discrete limit that transmission of modulated waves is described by the cubic-quintic complex Ginzburg-Landau equation.[14] Their work revealed that solitonlike excitations can be induced by MI. Recently, Abdoulkary *et al.* considered the dynamics of a dissipative discrete nonlinear electrical transmission line with negative nonlinear resistance and showed that the wave propagation is described by a generalized dissipative discrete complex Ginzburg–Landau equation.[15] They established the generalized discrete Lange–Newell criterion for MI phenomenon.

†Corresponding author. E-mail: fbpelap@yahoo.fr; francois.pelap@univ-dschang.org

© 2020 Chinese Physical Society and IOP Publishing Ltd

More recently, Doka used a dissipative nonlinear transmission line analog of the microtubules protein structure to derive a nonlinear lattice equation governing the voltage motion in the system.[16] Through the continuum approximation, he derived a nonlinear perturbed Korteweg–de-Vries (KdV) equation as the amplitude equation and studied theoretically the dynamics of its dark soliton solution. Next, one could easily note that very few investigations dealing with the nonlinear electrical bi-inductance transmission line (NLBTL) have been made. Within these studies[17–21] and to the best of our knowledge, no paper reports the dynamics of modulated waves in a dissipative NLBTL using the continuum approximation.

The outline of this paper is structured as follows. In Section 2, we present the model of discrete electrical bi-inductance transmission line with dissipative elements and find the differential difference equation governing its dynamics. In the low-amplitude limit (linear plane wave) of the voltage, the linear dispersion relation and the linear dissipative parameter of the damped oscillations are derived in Section 3. It appears that the system exhibits two modes of propagation: the low-frequency (LF) mode and the high-frequency (HF) mode. The effects of the linear dissipative coefficient on the frequency domain are checked. In Section 4, we consider the dynamics of the modulated waves in the continuum limit and recover the two modes of transmission. In Section 5, the dynamics of the modulated waves in the LF mode are deeply investigated and the complex Ginzburg–Landau equation is derived. The asymptotic behavior of the finite amplitude wave in this line is investigated and the impact of the dissipative factor is checked. The existence of both bright and dark solitons is established. Section 6 is devoted to discussion and concluding remarks.

2. Model description and basic equations

Consisting of N identical unit cells, our distributed dissipative NLBTL contains constant inductors (L_1, L_2) and voltage-dependant capacitors $C(V)$ as illustrated in Fig. 1. This network represents an electrical equivalent of a diatomic lattice in which atoms interact with their first nearest neighbors through an inter-atomic potential with cubic nonlinear interactions. Hereafter, the losses due to the resistances (r_1, r_2) of the inductors as well as the conductance $g_{\rm p}$ of the capacitances are taken into account in the study. By applying Kirchhoff's laws to the circuit of Fig. 1, we obtain the following set of fundamental equations:

$$\begin{cases} L_2 I_{2n-1,t} + r_2 I_{2n-1} = V_{2n-1} - V_{2n}, \\ L_1 I_{2n,t} + r_1 I_{2n} = V_{2n} - V_{2n+1}, \\ I_{g_{\rm p}2n} = V_{2n} g_{\rm p}, \end{cases} \quad \begin{cases} I_{g_{\rm p}2n+1} = V_{2n+1} g_{\rm p}, \\ Q_{2n,t} = I_{2n-1} - I_{2n} - I_{g_{\rm p}2n}, \\ Q_{2n+1,t} = I_{2n} - I_{2n+1} - I_{g_{\rm p}2n+1}, \end{cases} \tag{1}$$

in which $Q_{2n}(t)$ is the charge stored in the $2n$-th nonlinear capacitor biased by the dc voltage V_0; and I_{2n} stands for the current passing through the $2n$-th linear inductor with constant inductance L_1. The subscript t denotes the time differentiation. In Fig. 1, the nonlinear capacitor consists of a reverse-biased capacitance diode with differential capacitance $C(V_{2n}) = {\rm d}Q_{2n}/{\rm d}V_{2n}$ which is a nonlinear function of the voltage V_{2n}. For low voltages taken around V_0, the dependence $Q_{2n}(V_{2n})$ may be approximated by[17,18]

$$Q_{2n}(V_{2n}) \approx C_0 \left(V_{2n} - \alpha V_{2n}^2\right), \tag{2}$$

where the nonlinear parameter α and the characteristic capacitance $C_0 = C(V_0)$ are given respectively by[17,18] $\alpha = 0.159\ {\rm V}^{-1}$ and $C_0 = 540$ pF for $V_0 = 1.5$ V. Relation (2) is used to eliminate the current in systems (1). Computations lead to a system of $2N$ coupled nonlinear difference-differential equations, expressed in terms of the voltages V_{2n} and V_{2n+1}, that describes the evolution of the voltages along the dissipative bi-inductance transmission line,

$$\begin{cases} \left(V_{2n} - \alpha V_{2n}^2\right)_{tt} + Y_{r1}\left(V_{2n} - \alpha V_{2n}^2\right)_t + Y_{\rm rp} V_{2n,t} \\ = Y_2 \left(V_{2n-1} - V_{2n}\right) - Y_1 \left(V_{2n} - V_{2n+1}\right) - Y_{r1} Y_{\rm rp} V_{2n}, \\ \left(V_{2n+1} - \alpha V_{2n+1}^2\right)_{tt} + Y_{r2}\left(V_{2n+1} - \alpha V_{2n+1}^2\right)_t + Y_{\rm rp} V_{2n+1,t} \\ = Y_1 \left(V_{2n} - V_{2n+1}\right) - Y_2 \left(V_{2n+1} - V_{2n+2}\right) - Y_{r2} Y_{\rm rp} V_{2n+1}, \end{cases} \tag{3}$$

with $Y_1 = 1/L_1 C_0$, $Y_2 = 1/L_2 C_0$, $Y_{r1} = r_1/L_1$, $Y_{r2} = r_2/L_2$, and $Y_{\rm rp} = g_{\rm p}/C_0$. For convenience, we denote by $U_n(t)$ the voltage of the even cells (V_{2n}) with inductance L_2 and $W_n(t)$ the voltage of the odd cells (V_{2n-1}) with inductance L_1. Therefore, system (3) becomes

$$\begin{cases} \left(U_n - \alpha U_n^2\right)_{tt} + Y_{r1}\left(U_n - \alpha U_n^2\right)_t + Y_{\rm rp} U_{n,t} \\ = Y_2 \left(W_n - U_n\right) - Y_1 \left(U_n - W_{n+1}\right) - Y_{r1} Y_{\rm rp} U_n, \\ \left(W_{n+1} - \alpha W_{n+1}^2\right)_{tt} + Y_{r2}\left(W_{n+1} - \alpha W_{n+1}^2\right)_t + Y_{\rm rp} W_{n+1,t} \\ = Y_1 \left(U_n - W_{n+1}\right) - Y_2 \left(W_{n+1} - U_{n+1}\right) - Y_{r2} Y_{\rm rp} W_{n+1}, \end{cases} \tag{4}$$

with $n = 1, 2, \ldots, N$, where N is the number of cells considered in the network. We intend to solve this set of equations in the upcoming sections.

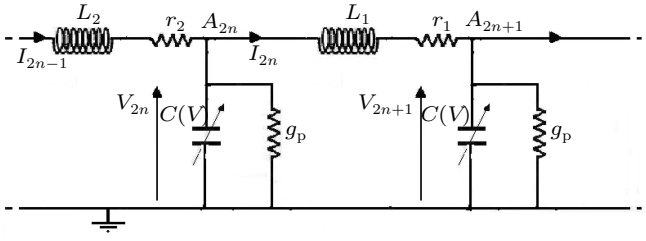


Fig. 1. One unit cell of the dissipative nonlinear bi-inductance transmission line. The network consists of N identical units.

3. Linear analysis of the network

This section examines the properties of the circuit of Fig. 1 in the linear domain. Consequently, the nonlinear parameter α no longer exists, the capacitance $C(V)$ becomes

constant and the stored charge is directly proportional to the voltage. Therefore, equation (2) is reduced to $Q_{2n}(U_n) \approx C_0 U_n$. However, these conditions do not affect the voltage range. The basic equation (4) characterizing the network takes the form

$$\begin{cases} (U_n)_{tt} + Y_{r1}(U_n)_t + Y_{\rm rp}U_{n,t} \\ = Y_2(W_n - U_n) - Y_1(U_n - W_{n+1}) - Y_{r1}Y_{\rm rp}U_n, \\ (W_{n+1})_{tt} + Y_{r2}(W_{n+1})_t + Y_{\rm rp}W_{n+1,t} \\ = Y_1(U_n - W_{n+1}) - Y_2(W_{n+1} - U_{n+1}) - Y_{r2}Y_{\rm rp}W_{n+1}. \end{cases} \tag{5}$$

Hereafter, we will examine the behavior of the plane waves travelling in the network. To consider the dissipative character of the lattice, we introduce a complex wave number $k = k_{\rm p} + {\rm i}\chi$ in which $k_{\rm p}$ and χ are, respectively, the wave number of the carrier wave and its linear dissipation coefficient. Let us mention that ${\rm i} = \sqrt{-1}$. Thus, the linear wave solutions of system (5) can be taken as

$$U_n(t) = B_2 \exp(-2n\chi) \exp\left[{\rm i}(2nk_{\rm p} - \omega t)\right] + {\rm c.c}, \tag{6a}$$

$$W_n(t) = B_1 \exp\left[-(2n-1)\chi\right] \exp\left\{{\rm i}\left[(2n-1)k_{\rm p} - \omega t\right]\right\} + {\rm c.c}, \tag{6b}$$

in which ω is the frequency of the carrier waves of amplitudes B_1 and B_2; c.c defines the complex conjugate of the preceding term since the signal voltage is real. Equation (6a) defines waves that evolve in cells with linear inductance L_2 and the grandeur (6b) corresponds to signals that propagate in the cells with linear inductance L_1. By substituting the voltages (6) into system (5) and retaining only the linear terms, one obtains a linear homogeneous system for B_1 and B_2,

$$\begin{cases} a\,B_1 + bB_2 = 0, \\ dB_1 + cB_2 = 0, \end{cases} \tag{7}$$

wherein $a = \omega^2 + Y_{r2}{\rm i}\omega + Y_{\rm rp}{\rm i}\omega - Y_t - Y_{r2}Y_{\rm rp}$; $b = Y_1 \exp(\chi - {\rm i}k_{\rm p}) + Y_2 \exp(-\chi + {\rm i}k_{\rm p})$; $Y_t = Y_1 + Y_2$; $c = \omega^2 + Y_{r1}{\rm i}\omega + Y_{\rm rp}{\rm i}\omega - Y_t - Y_{r1}Y_{\rm rp}$, and $d = Y_2 \exp(\chi - {\rm i}k_{\rm p}) + Y_1 \exp(-\chi + {\rm i}k_{\rm p})$.

The condition for the existence of nontrivial solutions of the homogeneous system (7) yields

$$\left\{\exp(2\chi)\cos(2k_{\rm p}) + \exp(-2\chi)\cos(2k_{\rm p}) + \frac{F_0}{D_0}\right\} + {\rm i}\left\{\exp(-2\chi)\sin(2k_{\rm p}) - \exp(2\chi)\sin(2k_{\rm p}) + \frac{G_0}{D_0}\right\} = 0, \tag{8}$$

with

$$\begin{aligned} D_0 &= -Y_1Y_2, \\ G_0 &= \omega^3\left[Y_{r1} + Y_{r2} + 2Y_{\rm rp}\right] \\ &\quad - \omega\left[2Y_{r1}Y_{r2}Y_{\rm rp} + Y_{r1}Y_{\rm rp}^2 + Y_{r2}Y_{\rm rp}^2 + Y_{r1}Y_t + Y_{r2}Y_t + 2Y_{\rm rp}Y_t\right], \\ F_0 &= \omega^4 - \omega^2\left[Y_{r1}Y_{r2} + 2Y_{r1}Y_{\rm rp} + 2Y_{r2}Y_{\rm rp} + Y_{\rm rp}^2 + 2Y_t\right] \\ &\quad + Y_{r1}Y_{r2}Y_{\rm rp}^2 + Y_{r1}Y_{\rm rp}Y_t + Y_{r2}Y_{\rm rp}Y_t - Y_1^2 - Y_2^2 + Y_t^2. \end{aligned}$$

Due to the uniqueness of the development of Eq. (8), the real part of this equation acts as the linear dispersion relation between $k_{\rm p}$ and ω, and its imaginary part may act as the linear dissipation equation for χ. We get from Eq. (8) the linear dispersion relation

$$\cos(2k_{\rm p}) = -\frac{F_0}{2D_0\cosh(2\chi)} \tag{9}$$

and the linear dissipation coefficient

$$\chi = 2^{-1}\ln\left(\vartheta + \sqrt{\vartheta^2 - 1}\right), \tag{10}$$

where the quantity ϑ is defined by

$$\vartheta = \sqrt{1 + \frac{(H_0^2 + I_0^2 - 1) - \left[(H_0^2 + I_0^2 + 1)^2 - 4H_0^2\right]^{1/2}}{2}}, \quad H_0 = -\frac{F_0}{2D_0}, \quad I_0 = \frac{G_0}{2D_0}. \tag{11}$$

In the absence of dissipation (i.e., $Y_{r1} = Y_{r2} = Y_{\rm rp} = 0$, then $\vartheta = 1$ and $\chi = 0$), the linear spectrum (9) is reduced to the well-known dispersion relation of the typical cut-band filter of the lossless nonlinear bi-inductance transmission line[17,18]

$$\omega^2 = \frac{1}{C_0}\left\{\left(\frac{1}{L_1} + \frac{1}{L_2}\right) \pm \sqrt{\left(\frac{1}{L_1} + \frac{1}{L_2}\right)^2 - \frac{4}{L_1L_2}\sin^2(k_{\rm p})}\right\}, \tag{12}$$

wherein the signs + and – refer, respectively, to the LF and HF modes of transmission. In the following, we focus our attention on the nonlinear behavior of the network. Therefore, equation (9) establishes the link between the wave number and the angular frequency in the general case of the dissipative bi-inductance transmission line.

Numerical resolution of Eq. (9) displays solutions plotted in Fig. 2. The curve of Fig. 2(a) exhibits all the existing solutions. Such mixed results were obtained by Essimbi *et al.*[22] during the study of a coupled nonlinear mono-inductance transmission line. From these results, we deduce the typical solution drawn in Fig. 2(b). This plot shows the existence of two modes of transmission in the dissipative NLBTL: the LF mode for frequencies $f \in [0, 1.835\ {\rm MHz}]$ and the HF mode for frequencies belonging to $[2.582\ {\rm MHz}, 3.186\ {\rm MHz}]$. These two modes are separated by a forbidden frequency domain [1.835 MHz, 2.582 MHz] that defines the gap zone of the system.

On the other hand, we check the behavior of the linear dissipation coefficient χ as function of the carrier wave frequency picked in the LF mode of transmission (Fig. 3). This graph shows that the dissipation (χ) grows as the carrier frequency increases. In the forthcoming sections, we analyze its impact on the other system parameters.

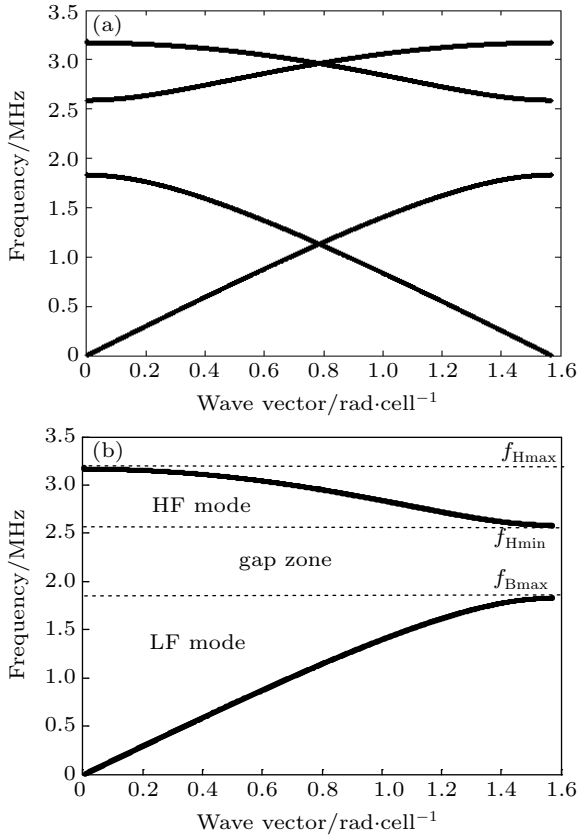


Fig. 2. Dispersion curves (versus the wave number k) of the carrier for the line parameters $L_1 = 28$ μH, $L_2 = 14$ μH, $V_0 = 1.5$ V, $C_0 = 540$ pF, $r_1 = 10^{-3}$ Ω, $r_2 = 0.5 \times 10^{-3}$ Ω, $g_{\rm p} = 10^{-7}$ S, and $\alpha = 0,159$ V^{-1}. (a) Various solutions of Eq. (9); (b) the simple symmetric solution of Eq. (9).

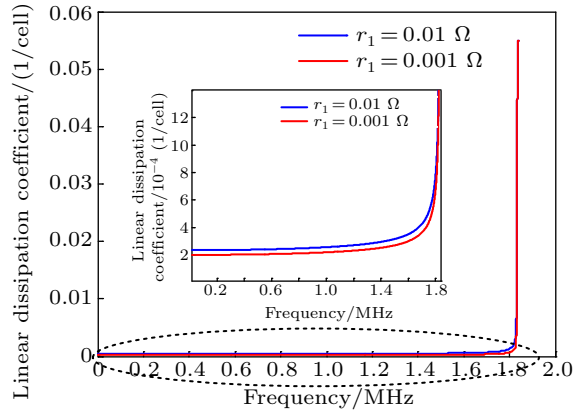


Fig. 3. Variation of the linear dissipation coefficient χ (cell^{-1}) in terms of the frequency f (MHz) chosen in the LF mode for various values of r_1.

4. Dynamics of modulated waves in the continuous approximation

Here, we start by presenting the mathematical approach used to examine the dynamics of modulated waves in the dissipative NLBTL using the continuous approximation (CA). To understand our motivations, we remind that Kofane *et al.*[17] established that the dynamics of nonlinear excitations in a lossless bi-inductance transmission line are described by a KdV-type equation. Recently, Pelap *et al.*[19] exploited the same network and demonstrated that the propagation of modulated waves in the CA is governed by a complex Ginzburg–Landau (CGL) equation. These results $(P_i, Q_i \neq 0)$ show that the bi-inductance line seems to generate damped dispersion and nonlinearity. To further understand the occurrence of this phenomenon, we plan to use the CA and deeply analyze the behavior of modulated excitations in the dissipative NLBTL by soliciting analytical techniques developed for diatomic chains.[23] Therefore, by applying the CA for the voltage of each inductance separately (i.e., if we set $x = 2n$), one obtains the upcoming expansions for $U_{n\pm1}$ and $W_{n\pm1}$ in terms of the Taylor series

$$U_{n\pm1} = U \pm 2\varepsilon\frac{\partial U}{\partial x} + 2\varepsilon^2\frac{\partial^2 U}{\partial x^2} \pm \frac{4}{3}\varepsilon^3\frac{\partial^3 U}{\partial x^3} + \frac{2}{3}\varepsilon^4\frac{\partial^4 U}{\partial x^4} \pm \frac{4}{15}\varepsilon^5\frac{\partial^5 U}{\partial x^5} + \frac{4}{45}\varepsilon^6\frac{\partial^6 U}{\partial x^6} + O\left(\varepsilon^7\right), \tag{13a}$$

$$W_{n\pm1} = W \pm 2\varepsilon\frac{\partial W}{\partial x} + 2\varepsilon^2\frac{\partial^2 W}{\partial x^2} \pm \frac{4}{3}\varepsilon^3\frac{\partial^3 W}{\partial x^3} + \frac{2}{3}\varepsilon^4\frac{\partial^4 W}{\partial x^4} + \frac{4}{15}\varepsilon^5\frac{\partial^5 W}{\partial x^5} + \frac{4}{45}\varepsilon^6\frac{\partial^6 W}{\partial x^6} + O\left(\varepsilon^7\right). \tag{13b}$$

In these relations, ε is a small scaling parameter such that $\partial/\partial t \sim O(\varepsilon)$, $\partial/\partial x \sim O(\varepsilon)$ which means that we are only interested in waves varying slowly in time and space. Within relations (13), the quantity 2ε measures the distance between two consecutive identical linear inductances. Based on relations (13), system (4) is transformed into two partial differential equations for $U(x,t)$ and $W(x,t)$,

$$\begin{aligned}&(U-\alpha U^2)_{tt} + Y_{r2}(U-\alpha U^2)_t + Y_{\rm rp}U_t\\ &= -Y_2(U-W) + Y_1(W_{n+1}-U) - Y_{r2}Y_{\rm rp}U,\end{aligned} \tag{14a}$$

$$\begin{aligned}&(W-\alpha W^2)_{tt} + Y_{r1}(W-\alpha W^2)_t + Y_{\rm rp}W_t\\ &= Y_2(U-W) - Y_1(W-U_{n+1}) - Y_{r1}Y_{\rm rp}W.\end{aligned} \tag{14b}$$

One could note that equations (14) are still coupled. To decouple them entirely, we call the following decoupling ansatz:[23]

$$W = \sigma\left[U + \varepsilon b_1 U_x + \frac{1}{2}\varepsilon^2 b_2 U_{2x} + \frac{1}{6}\varepsilon^3 b_3 U_{3x} + \frac{1}{24}\varepsilon^4 b_4 U_{4x} + \frac{1}{120}\varepsilon^5 b_5 U_{5x} + \frac{1}{720}\varepsilon^6 b_6 U_{6x} + O\left(\varepsilon^7\right)\right], \tag{15}$$

in which σ and b_j $(j = 1,\ldots,6)$ are grandeurs to be determined. Substituting Eq. (15) into system (14) leads to

$$\begin{aligned}&\varepsilon^2(U-\alpha U^2)_{tt} + \varepsilon Y_{r2}(U-\alpha U^2)_t + \varepsilon Y_{\rm rp}U_t\\ &= AU + \varepsilon BU_x + \varepsilon^2 CU_{2x} + \varepsilon^3 DU_{3x} + \varepsilon^4 EU_{4x}\\ &\quad + FU_{5x} + GU_{6x},\end{aligned} \tag{16a}$$

$$\begin{aligned}&\varepsilon^2(W-\alpha W^2)_{tt} + \varepsilon Y_{r1}(W-\alpha W^2)_t + \varepsilon Y_{\rm rp}W_t\\ &= A'U + \varepsilon B'U_x + \varepsilon^2 C'U_{2x} + \varepsilon^3 D'U_{3x} + \varepsilon^4 E'U_{4x}\\ &\quad + F'U_{5x} + G'U_{6x},\end{aligned} \tag{16b}$$

in which the diverse parameters are defined in Appendix A. The left hand sides of Eqs. (16a) and (16b) have the same shapes with the proper characteristics (L_2, r_2), (resp. (L_1, r_1))

that are related to the nature of the wave $U(x,t)$, (resp. $W(x,t)$) in each cell. If the right hand sides of these two equations are identical, then one could exploit either expression (16a) for $U(x,t)$ or relation (16b) for $W(x,t)$ to examine the dynamics of the signal in the network. For this to occur, the upcoming equivalences should be satisfied for the linear terms:

$$A = A', \tag{17a}$$
$$B = B', \tag{17b}$$
$$C = C', \tag{17c}$$
$$D = D', \tag{17d}$$
$$E = E', \tag{17e}$$
$$F = F', \tag{17f}$$
$$G = G'. \tag{17g}$$

The resolution of Eqs. (17) helps to complete information about our system. Indeed, from Eq. (17a), we obtain two values of σ,

$$\sigma = \pm 1. \tag{18}$$

The value $\sigma = +1$ deals with the LF mode of propagation where the voltages U and W, in one unit cell, are in phase whereas the value $\sigma = -1$ links to the HF mode of transmission where the two voltages are opposite in phase. Hereafter, we investigate the dynamics of the network in the LF mode of transmission.

5. Wave dynamics in the low frequency mode

5.1. Amplitude equation

In this subsection, the behavior of modulated excitations along the dissipative NLBTL is investigated in the LF mode of transmission which deals with $\sigma = +1$. For this value of σ, we solve Eqs. (17b)–(17g) by keeping terms up to $O(\varepsilon^7)$ and obtain respectively

$$\begin{aligned}
&b_1 = 2L/L_1;\ \ b_2 = 4L^2/L_1^2 = b_1^2;\\
&b_3 = 3b_1^3 - 6b_1^2 + 4b_1;\ \ b_4 = 9b_1^4 - 24b_1^3 + 16b_1^2;\\
&b_5 = 45b_1^5 - 180b_1^4 + 240b_1^3 - 120b_1^2 + 16b_1;\\
&b_6 = -b_{61}/b_{62},
\end{aligned} \tag{19}$$

with

$$b_{61} = 128Y_1\left(225Y_1^5 - 540Y_1^4Y_t + 450Y_1^3Y_t^2 - 150Y_1^2Y_t^3 + 16Y_1Y_t^4\right),$$

$$b_{62} = Y_t^5\left(Y_tY_{r2}Y_{\rm rp} - Y_{r1}Y_{\rm rp} - 2Y_t\right).$$

The report of expressions (19) into system (16) provides a single equation for $U(x,t)$ (or $W(x,t)$) which includes the influence of cells of the other rank (odd or even) owing to the starting considerations, namely,

$$U_{tt} - \alpha\left(U^2\right)_{tt} + \alpha Y_{r2}U_t^2 = AU + CU_{2x} + EU_{4x} + GU_{6x} + HU_t, \tag{20}$$

where

$$\begin{aligned}
&A = -Y_{r2}Y_{\rm rp};\ \ C = -2Y_1\left(4Y_1^2 - Y_1Y_t - Y_t^2\right)/Y_t^2;\\
&B = D = F = 0;\ \ H = -Y_{r2} - Y_{\rm rp};\\
&E = \frac{b_4}{24}Y_t - \frac{b_3}{3}Y_1 + b_2Y_1 - \frac{4}{3}b_1Y_1 + \frac{2}{3}Y_1,\\
&G = \frac{b_5}{120}Y_t - \frac{b_4}{12}Y_1 + \frac{b_3}{3}Y_1 - \frac{2}{3}b_2Y_1 + \frac{2}{3}b_1Y_1 - \frac{4}{15}Y_1.
\end{aligned}$$

Relation (20) is a damped Boussinesq-type equation for the voltage $U(x,t)$[24] in which the quantity C defines the velocity of the linear non dispersive waves and A, E, G, H are positive constants. In the limit case dealing with $L_1 = L_2 = L$, $r_1 = r_2 = 0$, and $g_{\rm p} = 0$, equation (20) is reduced to the well-known Boussinesq equation $\left(U - aU^2\right)_{tt} = C\left(U_{2x} + U_{4x}/12\right)$ with $C = 1/L$ that describes the wave propagation in the mono-inductance line.[25] With some suitable transformation, equation (20) can be reduced to the KdV equation.[17]

Instead of looking for the pulse solutions characteristic of the KdV systems,[17] we seek but the possible modulated wave solutions of Eq. (20). For this purpose and owing to the slow variation of the voltage from one cell to another, we introduce the multiple scales method where x and t are scaled into independent variables $x_0, x_1, \ldots, x_n$ and $t_0, t_1, \ldots, t_n$, respectively, with $x_n = \varepsilon^n x$ and $t_n = \varepsilon^n t$. By assuming this expansion, equation (20) is transformed up to the second harmonic generation. For convenience, we introduce $U \to \varepsilon U_1$ and replace x_0, x_1 and t_0, t_1, respectively, by x, X and t, T. Then, expression (20) becomes

$$\begin{aligned}
&U_{1,tt} + 2\varepsilon U_{1,tT} + \varepsilon^2 U_{1,TT} - \alpha\{U_{1,tt}^2 + 2\varepsilon\left(U_1^2\right)_{tT}\\
&+\varepsilon^2\left(U_1^2\right)_{TT}\} + \alpha Y_{r2}\left\{\left(U_1^2\right)_t + \varepsilon\left(U_1^2\right)_T\right\}\\
&= AU_1 + C\left\{U_{1,2x} + 2\varepsilon U_{1,xX} + \varepsilon^2 U_{1,XX}\right\}\\
&+E\left\{U_{1,4x} + 4\varepsilon U_{1,3xX} + 6\varepsilon^2 U_{1,2x2X} + 4\varepsilon^3 U_{1,x3X} + \varepsilon^4 U_{1,4X}\right\}\\
&+G\{U_{1,6x} + 6\varepsilon U_{1,5xX} + 15\varepsilon^2 U_{1,4x2X} + 20\varepsilon^3 U_{1,3x3X}\\
&+15\varepsilon^4 U_{1,2x4X} + 6\varepsilon^5 U_{1,x5X} + \varepsilon^6 U_{1,6X}\} + HU_{1,t}.
\end{aligned} \tag{21}$$

The modulated wave solutions of Eq. (21) are taken in the general form[23]

$$\begin{aligned}
U_1 \ =\ &\varepsilon U_{11}(X,T)\exp\left[\mathrm{i}\left(kx - \omega t\right)\right] + \text{c.c} + \varepsilon^2 U_{20}(X,T)\\
&+\varepsilon^2 U_{22}(X,T)\exp\left[2\mathrm{i}\left(kx - \omega t\right)\right] + \text{c.c.}
\end{aligned} \tag{22}$$

in which c.c. stands for the complex conjugate of the preceding term; ω and k are, respectively, the angular frequency and the complex wave number ($k = k_{\rm p} + \mathrm{i}\chi$) of the carrier that satisfy the following complex relation:

$$\begin{aligned}
&\omega^2 + A + C(\chi^2 - k_{\rm p}^2) + E(\chi^4 - 6\chi^2k_{\rm p}^2 + k_{\rm p}^4)\\
&+G(\chi^6 - 15\chi^4k_{\rm p}^2 + 15\chi^2k_{\rm p}^4 - k_{\rm p}^6)\\
&+\mathrm{i}\left[-2C\chi k_{\rm p} + E(-4\chi^3k_{\rm p} + 4\chi k_{\rm p}^3)\right.\\
&\left.+G(-6\chi^5k_{\rm p} + 20\chi^3k_{\rm p}^3 - 6\chi k_{\rm p}^5) - H\omega\right] = 0.
\end{aligned} \tag{23}$$

Equation (23) leads both to the dispersion relation (9) and the

linear dissipative coefficient (10) for the low frequency mode of transmission. Now, we pursue by substituting the general voltage (22) into Eq. (21) and applying the secular conditions to the resulting equation. Therefore, the terms proportional to $\varepsilon^2 \exp\left[2\mathrm{i}(k_\mathrm{p}x-\omega t)\right]$ and $\varepsilon^4 \exp\left[0\mathrm{i}(k_\mathrm{p}x-\omega t)\right]$ permit to determine, respectively, the voltages

$$U_{22} = A_1 U_{11}^2, \quad U_{20} = A_2 |U_{11}|^2, \tag{24}$$

in which

$$A_1 = [4\alpha\omega - \mathrm{i}2\alpha Y_{r2}\omega]/D_1, \; A_2 = 2\alpha V_\mathrm{g}^2 \exp(-2\chi x)/\left(V_\mathrm{g}^2 - C\right),$$

with

$$\begin{aligned} D_1 \; &= 4\omega + A + 4C\left(\mathrm{i}k_\mathrm{p} - \chi\right)^2 + 16E\left(\mathrm{i}k_\mathrm{p} - \chi\right)^4 \\ &\quad + 64G\left(\mathrm{i}k_\mathrm{p} - \chi\right)^6 - 2\mathrm{i}\omega H. \end{aligned}$$

Then, we set $z = X - V_\mathrm{g}T$, $\tau = \varepsilon T$ and collect information from the third order terms of the first harmonic. It appears that the evolution of a packet wave in the LF mode of transmission in the network is governed by the dissipative CGL equation

$$\mathrm{i}\frac{\partial U_{11}}{\partial \tau} + P\frac{\partial^2 U_{11}}{\partial z^2} + Q|U_{11}|^2 U_{11} = \mathrm{i}JU_{11}. \tag{25}$$

Equation (25) is a basic model utilized to describe phase transitions and wave propagation in various systems.[26,27] In this expression, the factor J represents the intrinsic dissipation of the circuit that deals with the imperfection of the differential capacitance $C(V)$ and justifies the presence of the conductance g_p. Within Eq. (25), the dispersion coefficient $P = P_\mathrm{r} + \mathrm{i}P_\mathrm{i}$ and the nonlinear coefficient $Q = Q_\mathrm{r} + \mathrm{i}Q_\mathrm{i}$ are defined by

$$\begin{aligned} P = \frac{1}{2\omega}\Big\{ &-V_\mathrm{g}^2 + C + \beta_2^2 - 2\mathrm{i}\beta_2 V_\mathrm{g} + 6E\left(\mathrm{i}k_\mathrm{p} - \chi\right)^2 \\ &+ 15G\left(\mathrm{i}k_\mathrm{p} - \chi\right)^4\Big\}, \end{aligned} \tag{26a}$$

$$Q = \mathrm{i}\alpha\omega Y_{r2}A_2 - \alpha\omega\left[A_1 \exp(-2\chi x) + A_2\right], \tag{26b}$$

with

$$\beta_2 = \frac{K_0 H_{11} + K_1 H_{12}}{16\beta_1\left[H_{13} + \sqrt{K_0^2 + K_1^2}\right]},$$

wherein the other quantities are defined below:

$$\begin{aligned} K_0 \; &= -4G\chi^6 + 60G\chi^4 k_\mathrm{p}^2 - 60G\chi^2 k_\mathrm{p}^4 + 4Gk_\mathrm{p}^6 - 4E\chi^4 \\ &\quad + 24E\chi^2 k_\mathrm{p}^2 - 4Ek_\mathrm{p}^4 - 4C\chi^2 + 4Ck_\mathrm{p}^2 - H^2 - 4A, \\ K_1 \; &= 24G\chi^5 k_\mathrm{p} - 80G\chi^3 k_\mathrm{p}^3 + 24G\chi k_\mathrm{p}^5 + 16E\chi^3 k_\mathrm{p} \\ &\quad - 16E\chi k_\mathrm{p}^3 + 8C\chi k_\mathrm{p}, \\ H_{11} \; &= -24G\chi^5 + 240G\chi^3 k_\mathrm{p}^2 - 120G\chi k_\mathrm{p}^4 - 16E\chi^3 \\ &\quad + 48E\chi k_\mathrm{p}^2 - 8C\chi, \\ H_{12} \; &= 120G\chi^4 k_\mathrm{p} - 240G\chi^2 k_\mathrm{p}^3 + 24Gk_\mathrm{p}^5 + 48E\chi^3 k_\mathrm{p} \\ &\quad - 16Ek_\mathrm{p}^3 + 8Ck_\mathrm{p}, \\ H_{13} \; &= 48G\chi^4 k_\mathrm{p} - 480G\chi^3 k_\mathrm{p}^2 + 240G\chi k_\mathrm{p}^4 + 32E\chi^2 \\ &\quad - 96E\chi k_\mathrm{p}^2 + 16C\chi, \\ \beta_1 \; &= \frac{1}{4}\left(2\sqrt{K_0^2 + K_1^2} - 2K_0\right)^{1/2} + \frac{1}{4}H. \end{aligned}$$

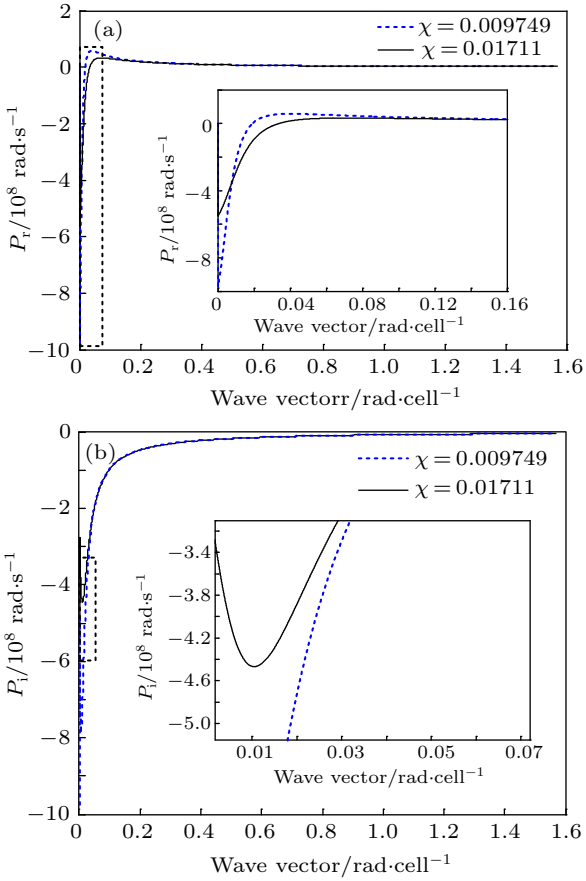


Fig. 4. Plots of the dispersion coefficient (P_r, P_i) in terms of k_p for the line parameters of Fig. 2 and several values of χ.

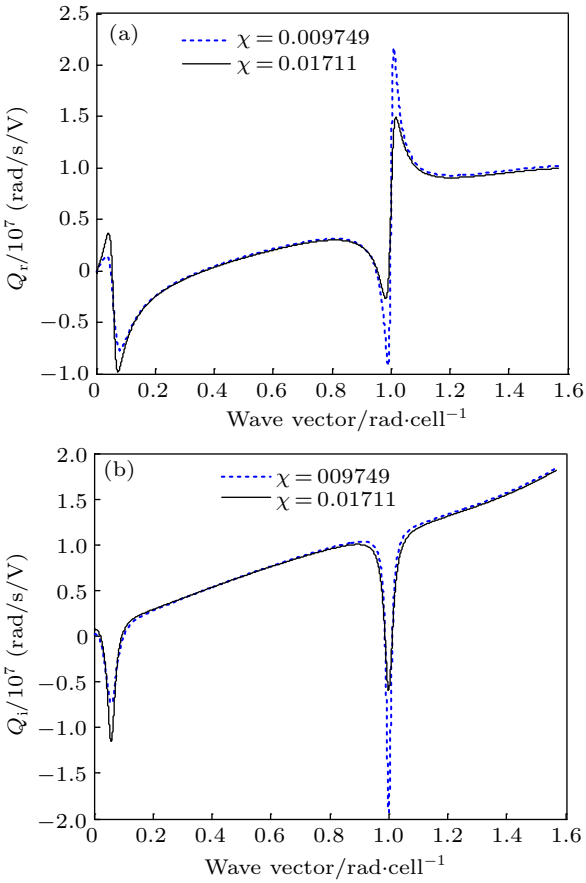


Fig. 5. Behavior of the nonlinear coefficient (Q_r, Q_i) versus k_p for the line parameters of Fig. 4. These plots show that those coefficients are non null.

5.2. Modulational instability

In modern nonlinear physics, modulational instability (or self-modulation) is considered as a basic process that classifies the qualitative behavior of modulated waves and may initialize the formation of stable entities such as envelope solitons.[28] The MI phenomenon informs on the asymptotic behavior of a plane wave during its evolution in a physical system. Pelap *et al.*[18] studied theoretically this phenomenon in a lossless bi-inductance transmission line and found that, in the low frequency mode, the plane wave remains stable under the modulation for wave numbers $k_{\rm p}$ lower than a critical value $k_{\rm c}$ and becomes unstable for values of $k_{\rm p}$ greater than $k_{\rm c}$. These authors showed that the MI phenomenon in the network is strongly linked to the sign of the pseudo product $P_{\rm r}Q_{\rm r}+P_{\rm i}Q_{\rm i}$. They established that a plane wave introduced in the lattice described by a complex Ginzburg–Landau equation is unstable under modulation if $P_{\rm r}Q_{\rm r}+P_{\rm i}Q_{\rm i}$ is positive and modulationally stable otherwise. These results were recovered by other researchers.[29] Now, we investigate the MI phenomenon in a dissipative NLBTL made of inductors and capacitors considered in a real experimental environment. Since the amplitude equation (25) is a CGL-type, we will use the existing results to examine the MI instability phenomenon in the network of Fig. 1. Then, the behavior of this pseudo product in terms of the carrier wave number for the dissipative model is scrutinized (Fig. 6). This curve shows that $P_{\rm r}Q_{\rm r}+P_{\rm i}Q_{\rm i}$ changes its sign for particular values of $k_{\rm p}$ chosen in the first Brillouin zone $(0\leqslant k_{\rm p}\leqslant \pi/2)$ and for the linear dissipation factor taken as $\chi=0.09749$. This plot also exhibits the existence of five regions concerning the modulational behavior of plane wave in the network (Fig. 6) and possible soliton solutions of Eq. (25).[18,30] Details are given below.

In region I, the carrier wave number $k_{\rm p}$ is in the range $0\leqslant k_{\rm p}\leqslant k_1$ with $k_1=0.01533$ rad·cell^{-1} that corresponds to the frequency domain $f\in[0,f_1]$ with $f_1=22.4$ kHz. Here, the pseudo product $P_{\rm r}Q_{\rm r}+P_{\rm i}Q_{\rm i}$ is always negative and a plane wave travelling in the line is modulationally stable. It appears from the results established in Refs. [18,30] that equation (25) admits a dark soliton solution.

In region II, the wave number $k_{\rm p}$ belongs to $k_1\leqslant k_{\rm p}\leqslant k_2$ with $k_2=0.08072$ rad·cell^{-1}. Since $P_{\rm r}Q_{\rm r}+P_{\rm i}Q_{\rm i}>0$ in this region, a plane wave moving in the lattice with a frequency f belonging to $[f_1,f_2]$ with $f_2=119.5$ kHz is unstable under modulation and, equation (25) possesses an envelope soliton solution.[18,30]

In region III, the carrier wave number $k_{\rm p}$ and frequency f are chosen in the ranges $k_2\leqslant k_{\rm p}\leqslant k_3$ and $f\in[f_2,f_3]$, respectively, with $k_3=0.99$ rad·cell^{-1} and $f_3=1390$ kHz. Within this region, we have $P_{\rm r}Q_{\rm r}+P_{\rm i}Q_{\rm i}<0$ and any plane wave introduced in the line is stable under modulation. Then, the amplitude wave equation (25) admits a hole soliton solution.[18,30]

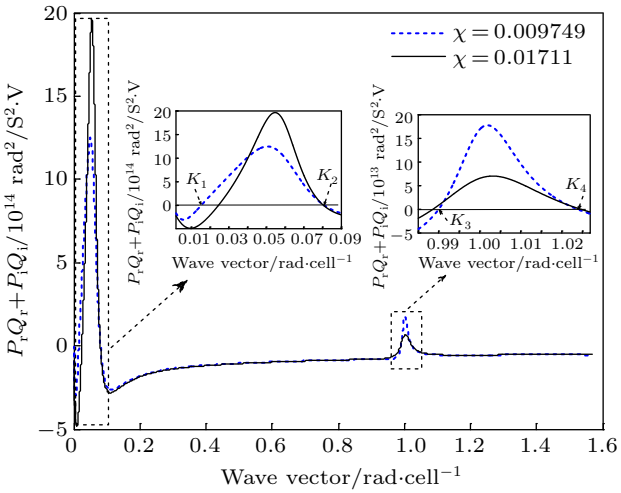


Fig. 6. Evolution of the pseudo product $P_{\rm r}Q_{\rm r}+P_{\rm i}Q_{\rm i}$ as a function of $k_{\rm p}$ in the LF mode with the parameters of Fig. 4. It appears that $P_{\rm r}Q_{\rm r}+P_{\rm i}Q_{\rm i}$ changes its sign for particular values of the wave number. These critical wave numbers are $k_1=0.01533$ rad·cell^{-1}, $k_2=0.08072$ rad·cell^{-1}, $k_3=0.99$ rad·cell^{-1}, and $k_4=1.025$ rad·cell^{-1}.

In region IV, we have $k_{\rm p}\in[k_3,k_4]$ with $k_4=1.025$ rad·cell^{-1}. Here, the pseudo product $P_{\rm r}Q_{\rm r}+P_{\rm i}Q_{\rm i}$ is always positive and a plane wave evolving in the network with a frequency f belonging to $[f_3,f_4]$ with $f_4=1432$ kHz is modulationally unstable and equation (25) has a bright soliton solution.[18,30]

In region V, the carrier wave characteristics $(k_{\rm p},f)$ belong to $k_4\leqslant k_{\rm p}\leqslant\pi/2$ and $f\in[f_4,f_{B\max}]$, respectively. Here, we have $P_{\rm r}Q_{\rm r}+P_{\rm i}Q_{\rm i}<0$ that deals with the modulational stability of a plane wave moving in the system and a hole soliton solution for the amplitude equation (25).[18,30]

These results are summarized on the dispersion curve of Fig. 7. As we can observe, this curve possesses five regions of modulational phenomena depending on the sign of $P_{\rm r}Q_{\rm r}+P_{\rm i}Q_{\rm i}$

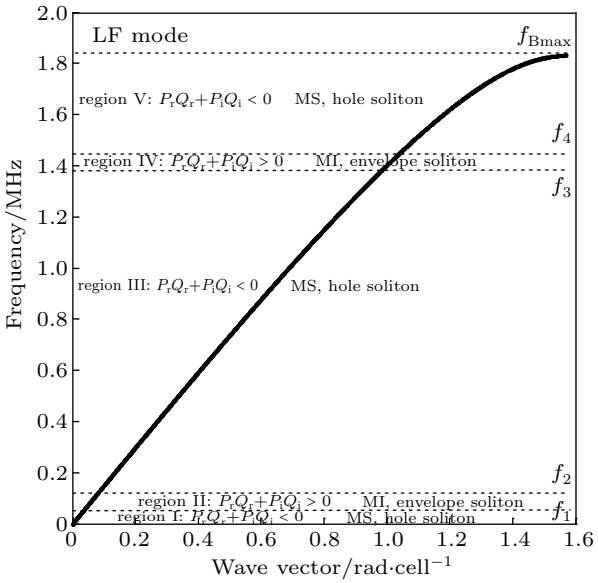


Fig. 7. Dispersion curve with a frequency band divided into five domains linking with the stability of the system and depending on the sign of the pseudo product $P_{\rm r}Q_{\rm r}+P_{\rm i}Q_{\rm i}$. The critical frequencies of the carrier are $f_1=22.4$ kHz, $f_2=119.5$ kHz, $f_3=1390$ kHz, and $f_4=1432$ kHz. Previous finding[21] displays only two domains of frequency in the LF mode.

instead of two regions as established in Ref. [21] for the lossless model. The solitary waves and the asymptotic behavior of plane waves expected theoretically in each region are stressed. It also appears from Fig. 6 that increasing the dissipation factor modifies the values of the wave numbers k_1 and k_3 but does not modify the number of modulational regions which remains equal to five. In the forthcoming section, we take a step towards experiment by doing numerical simulations.

5.3. Implementation and simulations

The entire simulation system is implemented and simulated by means of the professional LT-Spice software using realistic components for circuit simulations (Fig. 8). Similar experiment that exhibits very good results was recently carried out on the one-dimensional (1D) mono-inductance nonlinear transmission line.[31] The network has 58 identical unit cells. Each cell contains two diodes BB112 biased by a dc voltage $V_p = 1,5$ V through a resistance $r_d = 5$ MΩ. The linear capacitors C_c and C_{osc} are used to block the dc biased current but have no effect on the frequencies range. The linear resistor R_f is also introduced to protect the SRC generator. The linear inductors $L_1 = 28$ μH and $L_2 = 14$ μH possess associated resistances r_1 and r_2, respectively. The conductance of the differential diode is linked to the resistance r_p ($g_p = 1/r_p$). The sine waves are created in the programmable electronic generator (PEG) and the waveforms are observed and stored in the numerical oscilloscope XSC1.

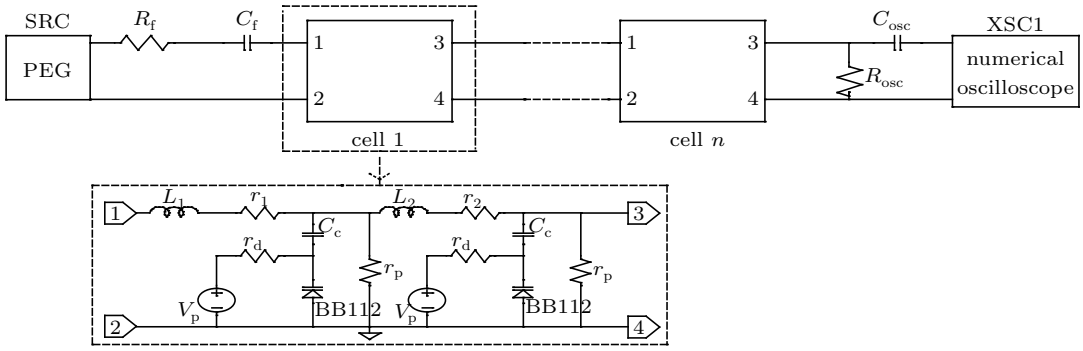


Fig. 8. Representation of the global simulation system.

To build the numerical results, the frequency of each wave is chosen in the different regions of the LF mode of transmission depicted in Fig. 7. To analyze numerically the MI phenomenon in the dissipative NLBTL, a plane wave generated by the PEG with desired characteristics is directly injected in the first cell of the line and its asymptotic behavior is watched in cells 1, 30, 41, 56 arbitrary chosen. The obtained results are displayed in Figs. 9–12 with the carrier wave frequencies taken, respectively, in regions I, III, IV, and V.

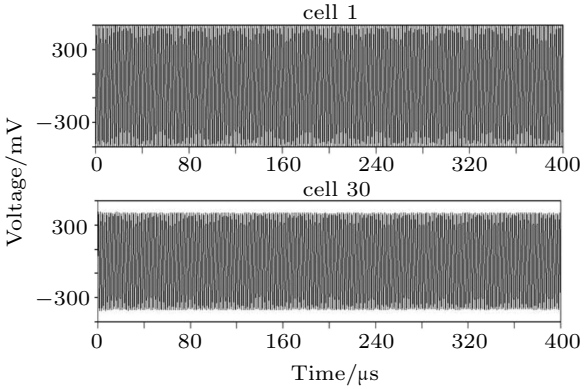


Fig. 9. Evolution of the signal voltage versus time exhibiting stability of a plane wave of frequency $f_p = 19,7$ kHz chosen in region I of the dispersion curve.

It appears from Figs. 9, 10, and 12 that after a slide adaptation to the line, the plane waves propagate without modulation. Furthermore, one observes the attenuation of the signal amplitude by about 5.5% in cell 30 and around 12% in cell 56 compared to the initial wave. On the other hand, figure 11 displays a signal unstable under modulation during its motion in the line. These curves show that the dissipation induces the decrement of the signal amplitude during the MI phenomenon. All these results are in perfect agreement with our analytical predictions.

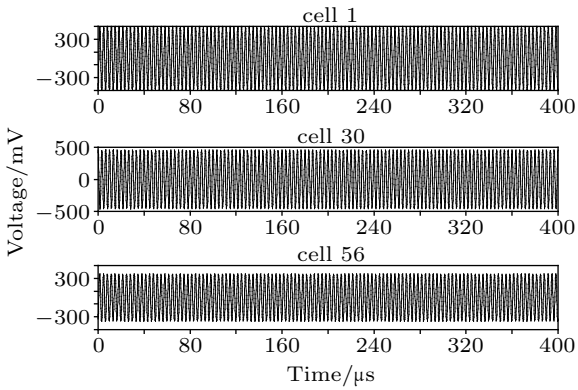


Fig. 10. Modulational stability of the plane wave of amplitude $A_p = 500$ mV and frequency $f_p = 300$ kHz belonging to region III. We could observe the attenuation of the signal amplitude by about 5.5% in cell 30 and 12% in cell 56 during its motion in the network.

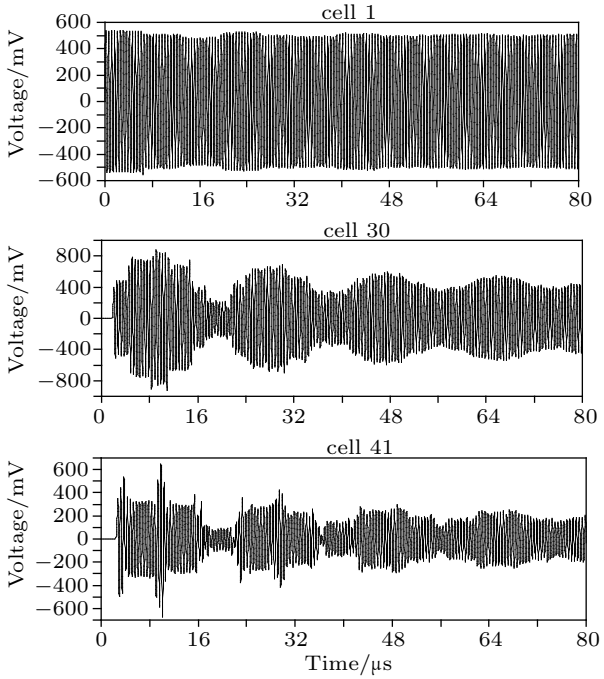


Fig. 11. Modulational instability of the plane wave with frequency $f_p = 1420$ kHz (region IV).

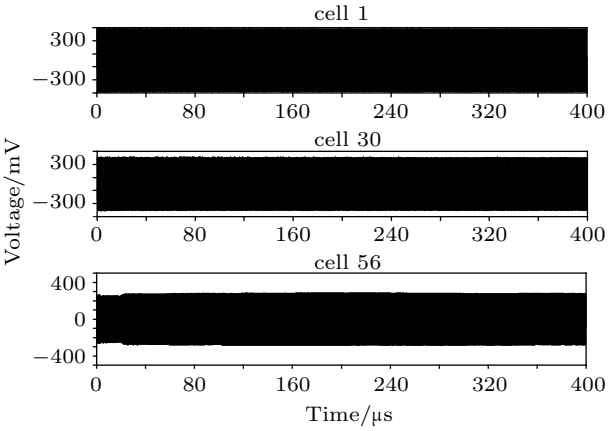


Fig. 12. Signal voltage in terms of time displaying stability of the plane wave for the frequency $f_p = 1673$ kHz taken in region V.

It should be mentioned that in region II, we observe modulational stability phenomenon instead of the modulational instability behavior predicted by the theory. This situation is probably due to the small frequency width of region II, which is comprised between two regions of modulational stability.

To experience the propagation of solitons in the dissipative NLBTL of Fig. 1, we subsequently adjust the PEG to deliver an envelope soliton with characteristics $A_p = 500$ mV, $f_p = 1420$ kHz, $f_m = 875$ kHz, and $m = 1$,[31] where A_p, f_p, f_m, and m are the amplitude, the carrier frequency, the modulation frequency, and the modulation index, respectively. We also adjust the PEG to generate a dark soliton with parameters $A_p = 500$ mV, $f_m = 875$ kHz, $m = 0.66$, and $f_p = 562$ kHz or $f_p = 1673$ kHz. The frequency of the carrier wave belongs to region I, III, IV, or V. Cells 1, 16, 32, 48 are arbitrarily picked to seek the behaviors of the input waves. Figures 13 and 15 exhibit the attenuated motion of the hole soliton in the network while figure 14 depicts the same behavior but for a bright soliton.

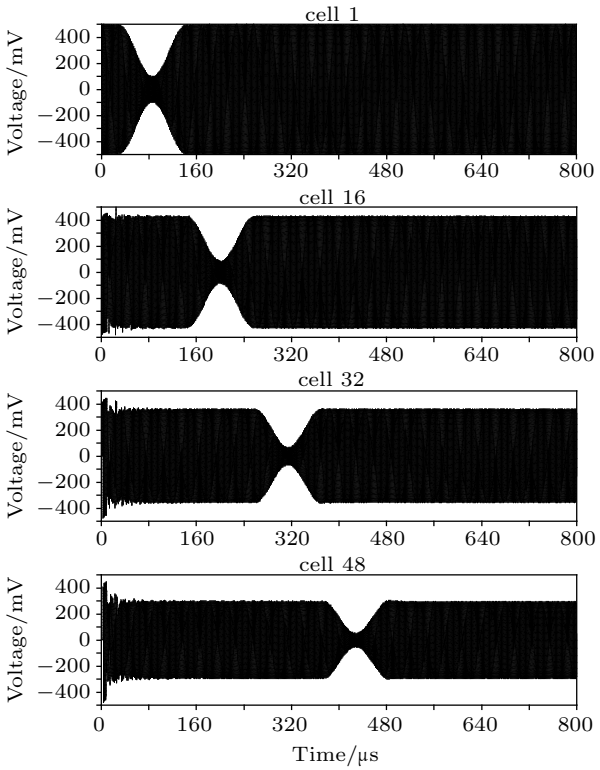


Fig. 13. Transmission of the dark soliton generated by the PEG with the characteristics $A_p = 500$ mV, $f_m = 875$ kHz, $m = 0.66$, and $f_p = 562$ kHz (region III) throughout the network of Fig. 8. We observe the propagation of the hole with diminution of its amplitude.

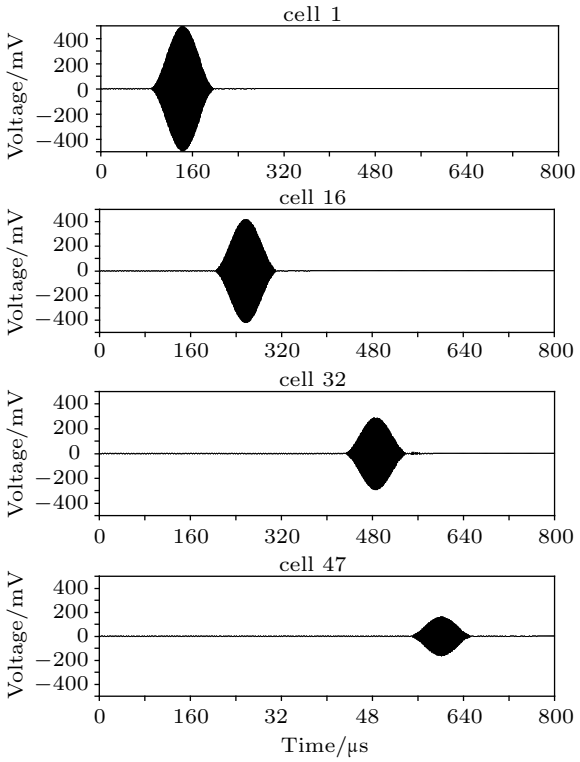


Fig. 14. Propagation of the bright soliton generated by the PEG with the parameters of Fig. 13 for $f_p = 1420$ kHz (region IV). The signal moves in the lattice with attenuation of its amplitude due to the dissipation.

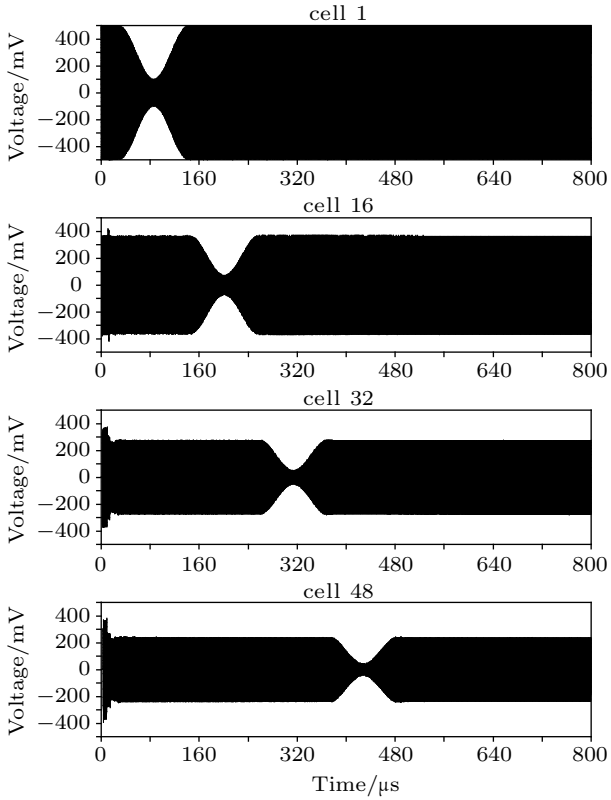


Fig. 15. Dissipative motion of the hole soliton issue from the PEG in the lattice with the parameters of Fig. 13 for $f_p = 1673$ kHz (region V).

6. Conclusion

We have studied analytically and numerically the dynamics of modulated waves in a nonlinear dissipative biinductance transmission line. The characteristic equation governing the propagation of the voltage propagation in the system was derived. In the linear limit, we have found that the network supports two propagation modes and carried out intensive investigations for the low frequency mode. We have shown that the dissipative effects increase with the frequency of the carrier wave. In the continuous approximation, we have established that the propagation of the modulated waves in the line is described by the complex Ginzburg–Landau equation instead of the Korteweg–de-Vries equation as usually known. While examining the asymptotic behavior of a plane wave traveling in the dissipative NLBTL, we obtained five regions of modulational phenomenon instead of two as previously established[18] for the LF mode of the lossless NLBTL. Moreover, plane waves generated by the PEG allowed the numerical observation of the modulational behavior in these different regions. Furthermore, an emphasis was made on the MI predicted analytically in region II which was not observed numerically. This may be due to the small frequency width of this region. Finally, we observed numerically the damped transmission of the bright and dark LF solitons generated by the PEG in the network. The numerical results obtained are in perfect agreement with the analytical predictions. Nevertheless, work is underway to examine the wave dynamics in the high frequency mode of the dissipative NLBTL.

Appendix A: Parameters of Eqs. (16a) and (16b)

$$A = Y_t(\sigma-1) - Y_{r2}Y_{\rm rp}; \quad B = \sigma(b_1Y_t - 2Y_1);$$

$$C = \sigma\left(\frac{b_2}{2}Y_t - 2b_1Y_1 + 2Y_1\right);$$

$$D = \sigma\left(\frac{b_3}{6}Y_t - b_2Y_1 + 2b_1Y_1 - \frac{4}{3}Y_1\right);$$

$$E = \sigma\left(\frac{b_4}{24}Y_t - \frac{b_3}{3}Y_1 + b_2Y_1 - \frac{4}{3}b_1Y_1 + \frac{2}{3}Y_1\right);$$

$$F = \sigma\left(\frac{b_5}{120}Y_t - \frac{b_4}{12}Y_1 + \frac{b_3}{3}Y_1 - \frac{2}{3}b_2Y_1 + \frac{2}{3}b_1Y_1 - \frac{4}{15}Y_1\right);$$

$$G = \sigma\left(\frac{b_5}{120}Y_t - \frac{b_4}{12}Y_1 + \frac{b_3}{3}Y_1 - \frac{2}{3}b_2Y_1 + \frac{2}{3}b_1Y_1 - \frac{4}{15}Y_1\right);$$

$$A' = -Y_t\frac{(\sigma-1)}{\sigma} - Y_{r1}Y_{\rm rp};$$

$$B' = -Ab_1 - b_1Y_t + \frac{2Y_1}{\sigma} - Y_{r1}Y_{\rm rp}b_1;$$

$$C' = -Bb_1 - A\frac{b_2}{2} - \frac{b_2}{2}Y_t + \frac{2Y_1}{\sigma} - Y_{r1}Y_{\rm rp}\frac{b_2}{2};$$

$$D' = -Cb_1 - B\frac{b_2}{2} - A\frac{b_3}{6} - \frac{b_3}{6}Y_t + \frac{4}{3}Y_1 - \frac{b_3}{6}Y_{r1}Y_{\rm rp};$$

$$E' = -Db_1 - C\frac{b_2}{2} - B\frac{b_3}{6} - A\frac{b_4}{24} - \frac{b_4}{24}Y_t + \frac{2}{3\sigma}Y_1 - \frac{b_4}{24}Y_{r1}Y_{\rm rp};$$

$$F' = -Eb_1 - D\frac{b_2}{2} - C\frac{b_3}{3} - B\frac{b_4}{24} - A\frac{b_5}{120} - \frac{b_5}{120}Y_t + \frac{4}{15\sigma}Y_1 - \frac{b_5}{120}Y_{r1}Y_{\rm rp};$$

$$G' = -Fb_1 - E\frac{b_2}{2} - D\frac{b_3}{6} - C\frac{b_4}{24} - B\frac{b_5}{120} - A\frac{b_6}{720} - \frac{b_6}{720}Y_t + \frac{4}{45\sigma}Y_1 - \frac{b_6}{720}Y_{r1}Y_{\rm rp}.$$

References

[1] Scott A 1999 *Emergence and dynamics of coherent structures, nonlinear science* (Oxford: Oxford University Press)

[2] Hirota R and Suzuki K 1970 *J. Phys. Soc. Jpn.* **28** 1366

[3] Afshari E and Hajimiri A 2005 *IEEE J. Solid State Circuits* **40** 744

[4] Albanese R, Penn J and Medina R 1993 *Ultrashort Pulse Response in Nonlinear Dispersive Media* (In *Ultra-Wideband, Short-Pulse Electromagnetics* edited by Bertoni H L, Carin L and Felsen L B) (Boston: Springer)

[5] Nejoh Y 1985 *Phys. Scr.* **31** 415

[6] Makenne Y L, Kengne R and Pelap F B 2019 *Chaos Soliton. Frac.* **127** 70

[7] Ndzana F I I and Mohamadou A 2019 *Chaos* **29** 013116

[8] Remoissenet M 1999 *Waves Called Solitons* 3rd Edn. (Berlin: Springer)

[9] Lonngren K E and Scott A C 1978 *Solitons in Action* (New York: Academic)

[10] Sarma A K and Saha M 2011 *J. Opt. Sc. Am. B.* **28** 944

[11] Agrawal G P 2007 *Nonlinear Fiber Opt.* 4th Edn. (San Diego: Academic Press)

[12] Pelap F B and Faye M M 2004 *J. Phys. A: Math. Gen.* **37** 1727

[13] Yemele D, Talla P K and Kofane T C 2003 *J. Phys. D.* **36** 1429

[14] Ndzana F I I, Mohamadou A and Kofane T C 2009 *Phys. Rev. E* **79** 047201
[15] Abdoulkary S, Beda T, Doka S Y, Ndzana F I I, Kavitha L and Mohamadou A 2012 *J. Mod. Phys.* **3** 438
[16] Doka S Y 2014 *J. Mod. Phys.* **5** 394
[17] Kofane T C, Michaux B and Remoissenet M 1988 *J. Phys. C: Solid State Phys.* **21** 1395
[18] Pelap F B, Kofane T C, Flytzanis N and Remoissenet M 2001 *J. Phys. Soc. Jpn.* **70** 2568
[19] Pelap F B and Faye M M 2007 *J. Phys. Soc. Jpn.* **76** 074602
[20] Kengne E and Vaillancourt R 2009 *Comm. Nonlin. Sc. Num. Sim.* **14** 3804
[21] Pelap F B, Tatsinkou I and Fomethe A 2011 *Phys. Scr.* **83** 045009
[22] Essimbi B Z, Ambassa L and Kofane T C 1997 *Physica D* **106** 207
[23] Tchawoua C, Kofane T C and Bokosah A S 1994 *Phys. Rev. B* **50** 4189
[24] Makhankov V G 1978 *Phys. Rep.* **35** 1
[25] Watanabe S 1982 *J. Phys. Soc. Jpn.* **51** 1030
[26] Miguel M S 1995 *Phys. Rev. Lett.* **75** 425
[27] Kengne E, Tadmon C and Vaillancourt R 2009 *Chin. J. Phys.* **47** 80
[28] Zakharov V E and Ostrovsky L A 2009 *Physica D* **238** 540
[29] Descalzi O, Martinez S and Tirapegui E 2001 *Chaos Soliton. Frac.* **12** 2619
[30] Nozaki K and Bekki N 1984 *J. Phys. Soc. Jpn.* **53** 1581
[31] Pelap F B, Kamga J H, Yamgoue S B, Ngounou S M and Ndecfo J E 2015 *Phys. Rev. E* **91** 022925